

Distributed Variational Quantum Algorithm with Many-qubit for Optimization Challenges

Seongmin Kim and In-Saeng Suh

National Center for Computational Sciences,

Oak Ridge National Laboratory, Oak Ridge, Tennessee 37830, United States.

Corresponding author. Email: kims@ornl.gov, suhi@ornl.gov

Optimization problems are critical across various domains, yet existing quantum algorithms, despite their great potential, struggle with scalability and accuracy due to excessive reliance on entanglement. To address these limitations, we propose variational quantum optimization algorithm (VQOA), which leverages many-qubit (MQ) operations in an ansatz solely employing quantum superposition, completely avoiding entanglement. This ansatz significantly reduces circuit complexity, enhances noise robustness, mitigates Barren Plateau issues, and enables efficient partitioning for highly complex large-scale optimization. Furthermore, we introduce distributed VQOA (DVQOA), which integrates high-performance computing with quantum computing to achieve superior performance across MQ systems and classical nodes. These features enable a significant acceleration of material optimization tasks (e.g., metamaterial design), achieving more than 50× speedup compared to state-of-the-art optimization algorithms. Additionally, DVQOA efficiently solves quantum chemistry problems and N -ary ($N \geq 2$) optimization problems involving higher-order interactions. These advantages establish DVQOA as a highly promising and versatile solver for real-world problems, demonstrating the practical utility of the quantum-classical approach.

Quantum computing leverages the principles of quantum mechanics to process information in ways fundamentally different from classical computing (1, 2). These unique properties provide a theoretical advantage for solving optimization problems, especially those formulated as energy minimization tasks on complex solution landscapes, where the goal is to find the ground state of a cost Hamiltonian (3, 4). Quantum algorithms excel in this domain by efficiently navigating the solution space, exploring multiple possibilities simultaneously, which classical computing cannot achieve (5, 6). This makes quantum computing particularly promising for combinatorial optimization problems, known as NP-hard (7). Variational quantum algorithms (VQAs), based on the variational principle (8) (Supplementary Text), have emerged as one of the most promising approaches to solving such problems by leveraging quantum computing (QC) in conjunction with classical computing (9, 10). VQAs combine parameterized quantum circuits (PQCs) with classical optimization: PQCs encode potential solutions while classical optimizers iteratively adjust the parameters to minimize a cost function (8, 11).

VQAs, such as quantum approximate optimization algorithm (QAOA), are primarily designed to handle binary optimization tasks, aligning with the binary nature of qubits (12–14). This inherently restricts their utility for N -ary optimization problems (e.g., ternary or quaternary tasks), where each variable assumes multiple states. This limits their applicability to broader optimization tasks that require multi-state variables. Moreover, VQAs face challenges when dealing with higher-order interactions, which involve interactions among multi-variables. Encoding these interactions requires numerous two-qubit entangling gates for quantum circuits, dramatically increasing circuit depth and computational complexity due to the combinatorial explosion in the number of two-qubit gates required as problem size increases (15, 16). Since two-qubit gates are prone to error and introduce computational overhead, this limits VQAs to efficiently solving higher-order problems (17–19). Consequently, for N -ary optimization problems involving higher-order (k^{th} -order) interactions, problem complexity scales as $O(N^m n^k)$ with n variables (Supplementary Text), making these problems extremely challenging. Therefore, a highly efficient ansatz with reduced algorithmic complexity is required to tackle such challenges.

Furthermore, VQAs may fail to reach the ground truth, especially for complex problems (8, 20, 21). This limitation can be mitigated by employing high-performance computing (HPC), which provides the computational capacity to explore broader solution spaces through distributed

computing (22). Although the integration of HPC and QC has great potential for addressing real-world problems (23), research on their integration to address these problems has been limited. This highlights the need for further investigation into how HPC can be optimally leveraged to enhance the performance of quantum algorithms, especially in improving solution quality by leveraging the strengths of both HPC and QC resources.

In this work, we present a variational quantum optimization algorithm (VQOA) designed to efficiently solve various real-world problems. VQOA features a highly efficient ansatz that relies solely on quantum superposition within a many-qubit (MQ) system (Fig. 1a), significantly reducing algorithmic complexity and computational cost. Here, MQ system refers to a quantum circuit system composed of numerous unentangled single-qubit rotation gates acting on many qubits, enabling a quantum-parallel approach. This MQ system enables seamless circuit partitioning without losing any quantum information, allowing for large-scale quantum simulations. Furthermore, this algorithm achieves superior performance by utilizing HPC-QC integrated systems (termed Distributed VQOA; “DVQOA”), demonstrating its capability to practically utilize quantum-centric supercomputing architectures. With these unique capabilities, DVQOA effectively addresses a wide range of real-world problems, including N -ary ($N \geq 2$) problems that involve higher-order ($k \geq 2$) interactions, highlighting the practical utility of the quantum-classical approach.

Efficient ansatz and circuit partitioning

The efficient ansatz is the core of VQOA, enabling remarkable scalability and adaptability for various optimization challenges. Conventional VQAs, such as QAOA, are designed to approximate the optimal solution of combinatorial optimization problems, but often rely on complex quantum circuits with numerous two-qubit entangling gates, which increase circuit depth and introduce significant errors (15, 24). The primary difference between QAOA and VQOA lies in their circuit design and parameter optimization. QAOA employs a variational ansatz consisting of alternating layers for a problem-specific cost Hamiltonian (H_C) and a mixing Hamiltonian (H_M), with each layer having two trainable parameters: one for the cost Hamiltonian and one for the mixing Hamiltonian. However, as problem size increases, QAOA faces significant challenges due to heavily entangled two-qubit gates (such as CNOT gates), leading to performance degradation caused by ac-

cumulated gate errors, decoherence, and hardware connectivity constraints. While these challenges may be mitigated in the future with the development of fault-tolerant quantum computers, their resolution remains contingent on advancements in quantum error correction and scalable quantum architectures.

In contrast, VQOA employs MQ system (i.e., an ansatz that entirely eliminates two-qubit gates, relying solely on single-qubit rotation gates), significantly reducing circuit complexity and minimizing noise effects (Fig. 1a). Each rotation gate has an independent parameter, optimized by a classical optimizer. The parameterized rotation gates naturally capture higher-order interactions among variables, enabling VQOA to execute considerably faster and more accurately than conventional VQAs. In VQOA’s ansatz, R_x and R_y gates are the effective gates to determine computational states after measurements on the z -basis (Fig. S1) (25). However, using both R_x and R_y gates unnecessarily increases the number of trainable parameters, potentially degrading performance. By exclusively using R_y gates, the circuit avoids unnecessary complexity while maintaining effectiveness. This simplified ansatz ensures that the interactions among variables can be effectively captured through parameter optimization without using entangling gates.

For executing VQOA on quantum hardware, the maximum number of iterations is constrained to 200 to manage quantum computing costs. While approximation ratios achieved on the IBM-Strasbourg quantum device and noiseless simulator may not reach the ground truth due to the constrained iterations, their overall performance remains comparable, demonstrating the algorithm’s robustness against errors introduced by hardware imperfections (Fig. 1b). This high performance on hardware is attributed to the exclusive use of error-robust single-qubit gates in the ansatz, highlighting the practicality of implementing this quantum algorithm on real quantum devices. Notably, quantum algorithm execution scales significantly differently between hardware and simulator. On hardware, execution time remains largely independent of circuit width (i.e., problem size, n), exhibiting constant time complexity. This demonstrates the suitability of quantum devices for tackling large-scale problems. In contrast, on the simulator, execution time grows exponentially with circuit width, as the simulator should classically track all possible quantum states and perform quantum operations accordingly (Fig. 1c, Supplementary Text) (26, 27).

Despite the demonstrated speedup on hardware, limited access to quantum device resources necessitates continued reliance on quantum simulators for research and development of quantum

algorithms. A key strength of our approach lies in the absence of two-qubit entangling gates, which enables seamless partitioning of quantum circuits without any loss of quantum information. This feature allows the circuit to be divided into smaller, independent segments, significantly enhancing scalability for large-scale quantum simulations. Partitioning the circuit greatly reduces the overall computational effort required to solve large problems while maintaining high approximation ratios. For example, solving problems ($n = 30$) without partitioning would require substantial computational time using a simulator. However, by partitioning the circuit into smaller pieces, the time to solution is exponentially reduced without compromising solution quality due to significantly reduced memory demand for simulations (Fig. S2). This indicates that single-qubit simulation is feasible, where each qubit is simulated independently, which results in a linear increase in time to solution with problem size (Fig. 1c). However, for moderately wide circuits, simulating the entire circuit without partitioning can be more efficient, highlighting the importance of optimizing the number of segments for efficient wide-circuit simulations (Fig. 1c). Furthermore, considering the time scaling of VQOA on quantum hardware and simulator, the results show that quantum algorithms may achieve computational speedup on quantum hardware over simulators beyond a certain problem size, even after circuit partitioning.

There are two key hyperparameters in the ansatz: the number of layers (m) and repeats (t). The hyperparameter m controls the number of trainable parameters in the circuit, while t repeats the circuit structure to enhance its expressive power, as illustrated in Fig. 1a. Excessively high values of m can lead to lower approximation ratios due to an unnecessary increase in the number of trainable parameters, but this issue can be efficiently mitigated by increasing t while keeping m small. Repeated rotation gates (t) enhance circuit complexity to explain complex solution spaces without excessively increasing the number of trainable parameters. VQAs often encounter challenges in identifying ground truth due to the Barren Plateaus phenomenon, where the gradient of the cost function diminishes exponentially, hindering effective optimization. This issue can be addressed by employing a reasonable number of trainable parameters with fewer entangling gates (28–30). By selecting an optimal number of trainable parameters without entanglement, our approach effectively avoids the Barren Plateaus problem, thereby resulting in improved approximation ratios (Fig. S3a,b,c). Here, increasing both m and t results in a linear increase in time to solution, leading to an algorithmic complexity of $O(nmt)$ (Fig. S3d,e,f). To balance computational efficiency and solution

quality, specific values of m and t are selected. For smaller problems ($n \leq 20$), they are set to 3, whereas they are set to 7 for larger problems ($n > 20$). These hyperparameters provide robust performance across a wide range of problem sizes while maintaining acceptable computational costs.

HPC-QC integration

In optimization, it is crucial to explore diverse regions of a solution space to find the global optimum. Integrating HPC with QC to leverage multi-cores/nodes can significantly enhance the solution quality by enabling distributed execution of quantum algorithms with varying initial parameters. This ensures comprehensive exploration of the solution space, increasing the chances of identifying the global optimum. Although increasing the number of cores (c) can introduce communication overhead, its impact on time to solution is modest. For instance, utilizing 500 cores results in only a $\sim 41\%$ increase in time to solution compared to using 10 cores, primarily due to variations in convergence speeds across executions (Fig. S4). These results highlight the practicality of distributed execution for achieving high-quality solutions while maintaining computational efficiency. Therefore, to maximize the solution quality, ideally approaching the ground truth, DVQOA employs 500 cores (with 10 compute nodes) for further studies.

Brute force search guarantees the identification of the ground truth (31). However, its runtime for quadratic unconstrained binary optimization (QUBO) problems increases exponentially with n , making it computationally challenging for large-scale problems. While utilizing multiple cores (c) can reduce computation time linearly, the overall time complexity remains exponential at $O(2^n/c)$ (Fig. S5). In contrast, DVQOA achieves significantly higher efficiency with a linear time complexity of $O(nmt)$, allowing it to find the ground truth substantially faster than brute force methods (Fig. 1d). However when the number of qubits does not divide evenly into the partition numbers, the approximation ratio may degrade. This issue can be simply mitigated by adjusting the number of partitions to ensure even distribution, which has minimal impact on the time (Fig. S6).

QAOA is widely used for tackling QUBO problems (8, 32). However, its reliance on many two-qubit operators in the cost layers leads to deep circuits, making QAOA inefficient in current quantum computing systems (quantum hardware and simulators) (15, 24). Consequently, QAOA

exhibits low approximation ratios and long time to solutions (Fig. 1e,f) (33). On the other hand, DVQOA features significantly shallow and efficient circuits, thus it can achieve much shorter time with higher approximation ratios. Moreover, DVQOA demonstrates robust scalability, effectively solving larger problems that QAOA struggles with ($n = 32, 36,$ and 40 ; Fig. S6). Note that DVQOA can be implemented on quantum-centric supercomputing architectures, utilizing either a single quantum device with qubit clusters or multiple quantum devices for distributed processing (Fig. S7).

Efficiency of DVQOA for real-world problems

DVQOA can be used for addressing various problems, simply redefining its cost function with the same ansatz (Fig. 2a). To demonstrate this, DVQOA is applied to solve Max-Cut problems, typical examples of binary combinatorial optimization (34). Their problem complexity grows exponentially with increasing number of nodes (Fig. S8) (7). Despite their complexity, DVQOA reliably converges to the ground truth, achieving approximation ratios of 1 (Fig. 2b). Similar to its performance on QUBO problems (Fig. S6), QAOA struggles with modest-scale Max-Cut problems (e.g., $n = 30$), yielding low approximation ratios and long time to solutions (Fig. S9). On the other hand, our quantum algorithm demonstrates remarkable scalability, solving problems with up to 1,000 nodes, which are far beyond the reach of brute force search and QAOA. For such large-scale Max-Cut problems, hybrid quantum annealing (HQA), one of the best solvers for these problems (Table S1) (7, 35, 36), is used as a reference for comparison. Although this experiment does not include distributed executions, our VQOA consistently achieves high approximation ratios (> 0.93) and maintains short times to solution ($< 1,000$ s) even without hyperparameter optimization for such scales (Fig. S10). Additionally, DVQOA demonstrates its versatility to handle other optimization problems, e.g., traveling salesman problems (TSP). It identifies the optimal routes with (near)-optimal distances, outperforming a classical solver (simulated annealing; SA) and achieving performance on par with a leading quantum solver (HQA) for these problems (Fig. 2c, Fig. S11, and Table S2).

It should be noted that DVQOA applies not only to optimization tasks but also to minimum eigenvalue calculation through cost function evaluation, e.g., computing the minimum eigenval-

ues of a Hamiltonian representing a molecule. Variational quantum eigensolver (VQE) with a two-local ansatz has been used for quantum chemistry to identify the minimum energy state of molecules (37, 38). While VQE with the two-local ansatz achieves high accuracy for simple molecular structures, such as hydrogen, its performance deteriorates for more complex systems, indicated by lower approximation ratios (Materials and Methods). In contrast, our algorithm, which exclusively employs single-qubit operators in the ansatz, consistently identifies low-energy states near the ground state across all studied chemical problems, demonstrating superior accuracy (Fig. 2d). These results clearly show DVQOA’s high performance not only in optimization but also in eigenvalue computations, reinforcing its broad applicability.

Importantly, DVQOA’s exceptional efficiency extends to material optimization tasks, such as layered photonic structures designed for energy-saving windows (Fig. S12, Materials and Methods) (39–41). Fig. 2e shows that DVQOA achieves convergence well, resulting in a highly optimized structure that outperforms the best-known result in the field. This optimized structure exhibits improved performance indicated by a lower figure-of-merit (FOM) (40). To further showcase DVQOA’s potential, it is employed to design metamaterial optical diodes, which aim to enable unidirectional light transmission (Fig. S13, Materials and Methods) (42, 43). The results in Fig. 2f reveal that DVQOA not only converges effectively but also identifies a structure with better performance than the best-known material (42).

These material optimization tasks are particularly challenging due to the exponential growth of the optimization space arising from the combinatorial explosion of possible configurations (40, 42, 44). Despite the inherent exponential problem complexity, DVQOA exhibits remarkable efficiency, requiring less than one second per iteration and completing the optimization of 40-qubit problems within ~25 minutes (Fig. 2g). This presents a significant acceleration of DVQOA (> 50×) compared to state-of-the-art quantum computing-assisted active learning algorithms designed for material optimization, which require ~1,342 minutes (33, 40, 42, 44). DVQOA achieves this speed by avoiding the need for surrogate modeling, a common approach in active learning algorithms to approximate optimization spaces (45, 46). Here, surrogate modeling introduces additional computational overhead, often requiring tens of seconds through machine learning techniques (45–47). In contrast, DVQOA inherently functions like a quantum active learning algorithm by directly leveraging its ansatz as a surrogate model to minimize the cost function, making it considerably

faster than other active learning algorithms. These results highlight DVQOA’s groundbreaking efficiency, particularly in material science, by significantly reducing computational time while achieving higher-quality outcomes. Furthermore, these demonstrate that DVQOA is not limited to QUBO-type problems but can effectively solve a broad range of real-world problems.

Higher-order (k^{th}) N -ary optimization challenges

DVQOA can inherently capture higher-order interactions among multi-variables, enabling it to capture more complex relationships during optimization. Table 1 proves DVQOA’s ability to accurately solve problems involving higher-order interactions ($k = 3, 4, \text{ and } 5$). This capability ensures the identification of superior optimization results with lower FOM values in material optimization tasks, compared to the active learning algorithms (Fig. 2e,f). Quantum solvers such as QA, HQA or QAOA, used in the active learning algorithms, are generally limited to handling 2^{nd} -order problems (33, 40, 42). This limitation prevents them from capturing the complexities of higher-order interactions (40, 42), leading to suboptimal outcomes. DVQOA’s enhanced capability overcomes these limitations, enabling it to achieve significantly better results. Furthermore, a performance comparison between DVQOA and a classical machine learning algorithm (distributed execution of deep neural networks, DDNN), presented in Table 1 and Table S3, reveals that DVQOA outperforms the DDNN, achieving higher approximation ratios and significantly shorter time to solutions, particularly for more challenging problems (Supplementary Text). These results demonstrate the advantage of utilizing the quantum approach over classical algorithms.

The inherent binary nature of qubits (12, 13), which represent states 0 and 1, poses challenges for conventional VQAs in modeling and optimizing N -ary problems. DVQOA overcomes this limitation by assigning multiple states on the Bloch Sphere to represent different labels (48). This approach maps a state vector to a specific label (Fig. 3a), allowing each qubit to represent one among multiple states (≥ 2), thereby enabling DVQOA to effectively solve N -ary optimization challenges. These N -ary problems, such as ternary or quaternary optimization, present exponentially larger solution spaces (3^n or 4^n) compared to binary optimization problems (2^n), making them significantly more challenging to solve. Additionally, the inclusion of higher-order interactions further increases the complexity, resulting in an exponential problem complexity of $O(N^n n^k)$ (Supplementary Text).

DVQOA can successfully solve such highly intricate problems with a linear complexity $O(nmt)$, reliably identifying the ground truth (Table S4). For these complex scenarios, hyperparameter tuning may be required to efficiently capture complex relationships for the identification of the ground truth (Table S4,5). Table 2 presents DVQOA’s exceptional capability to accurately solve N -ary optimization problems (binary, ternary, quaternary, and quinary) involving 2^{nd} and 3^{rd} -order interactions within a minute.

To further demonstrate DVQOA’s capability in solving N -ary optimization problems in material science, layered photonic structures are optimized where each layer can take one of three material candidates (ternary problem). While conventional methods require additional qubits and constraints to represent multiple states (40), DVQOA’s state-vector assignment on the Bloch sphere efficiently eliminates this requirement (48), leading to superior optimization results (Fig. 3b, Supplementary Text). Moreover, increasing m and t allows more parameter adjustments, resulting in further optimized structures with lower FOMs. As shown in Fig. S14, the optimized photonic structure exhibits improved optical characteristics. Fig. 3c presents a linear time complexity of DVQOA, demonstrating its scalability and efficiency in solving real-world multi-state problems. This exceptional performance of DVQOA makes it a unique and revolutionary tool to handle various optimization tasks across diverse domains.

Conclusion

We have proposed a highly efficient ansatz that relies exclusively on single-qubit gates, capturing interactions among multi-variables through parameter optimization. This approach allows quantum circuits to be seamlessly partitioned without loss of quantum information, enabling large-scale quantum simulations. The algorithm’s performance is significantly enhanced with high accuracy through distributed execution with diverse initial parameters on HPC-QC systems. The versatility to tackle various real-world problems including quantum chemistry calculations is another key advantage of DVQOA. Furthermore, DVQOA functions like quantum active learning, significantly accelerating (more than 50×) material optimization tasks and achieving superior results compared to state-of-the-art optimization algorithms. Remarkably, the algorithm extends beyond binary optimization by enabling multi-state optimization, where each qubit can represent multiple states on the

Bloch sphere. This highlights DVQOA's capability for effectively addressing higher-order N -ary optimization challenges. Importantly, our results demonstrate a practical advantage of utilizing the quantum approach in optimization, with quantum hardware exhibiting constant complexity and the quantum-classical algorithm outperforming well-established classical algorithms. These findings establish DVQOA as a powerful and versatile tool for solving challenging problems utilizing current QC technologies. Therefore, we expect that DVQOA will play a critical role in optimization and eigenvalue calculation across various fields. Moreover, this work lays the groundwork for leveraging near-term quantum devices in solving real-world challenges effectively.

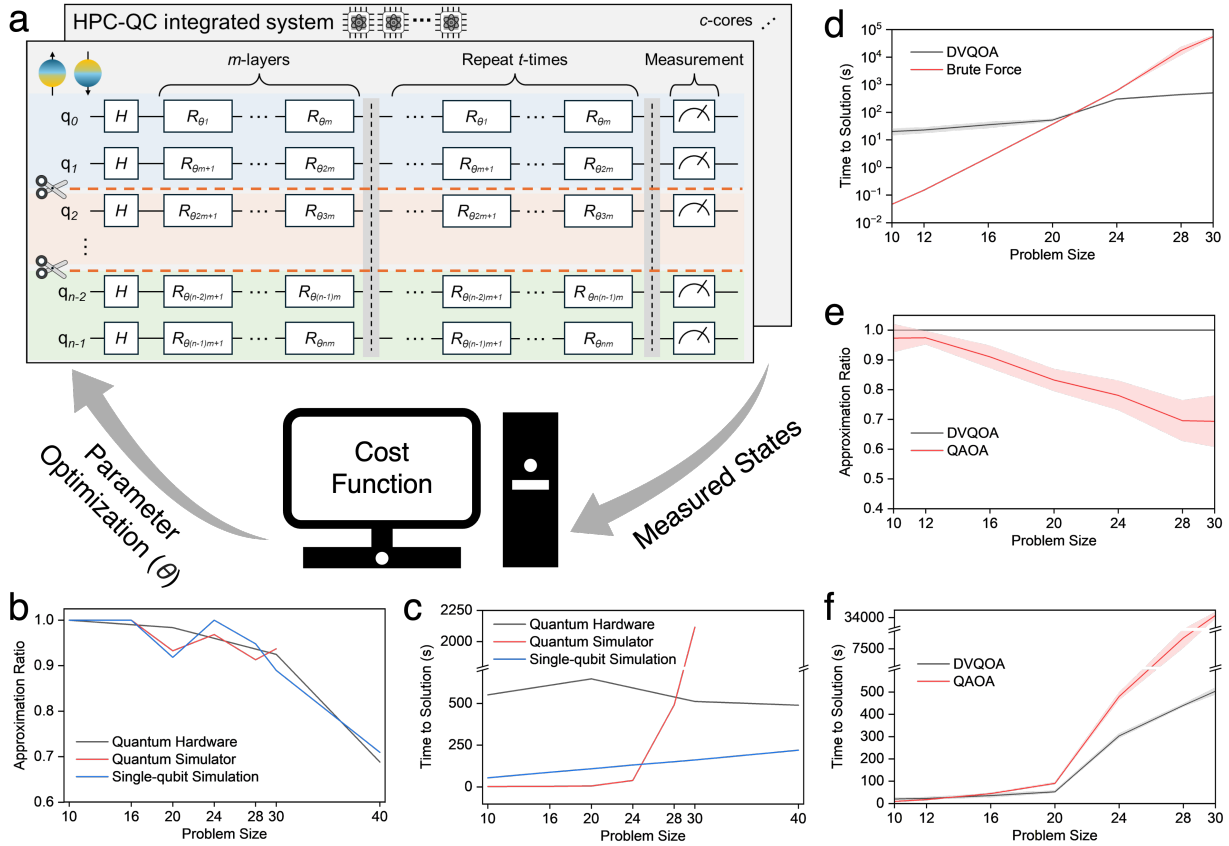


Figure 1: Workflow and performance of VQOA. **a**, Schematic representation of VQOA workflow, featuring the efficient ansatz and the iterative adjustment of rotation gate parameters through classical optimization to minimize the cost function. The problem size corresponds to circuit width (n), and HPC-QC integrated systems enable distributed executions of VQOAs (DVQOA). Approximation ratio (**b**) and time to solution (**c**) for VQOA on quantum hardware (IBM-Quantum-Device) and quantum simulator (Qiskit-Aer). Here, each qubit is simulated independently for single-qubit simulations. While quantum hardware maintains constant time complexity, the simulator exhibits exponential growth in the time, whereas single-qubit simulations scale linearly. **d**, Comparison of the time to solution between DVQOA and brute force. Brute force requires exponential time $O(2^n)$ to identify the ground truth as n increases, while DVQOA exhibits a linear algorithmic complexity. Approximation ratio (**e**) and time to solution (**f**) of DVQOA and QAOA for QUBO problems as a function of n . While QAOA shows degraded performance with increasing n , DVQOA maintains stable performance across varying n .

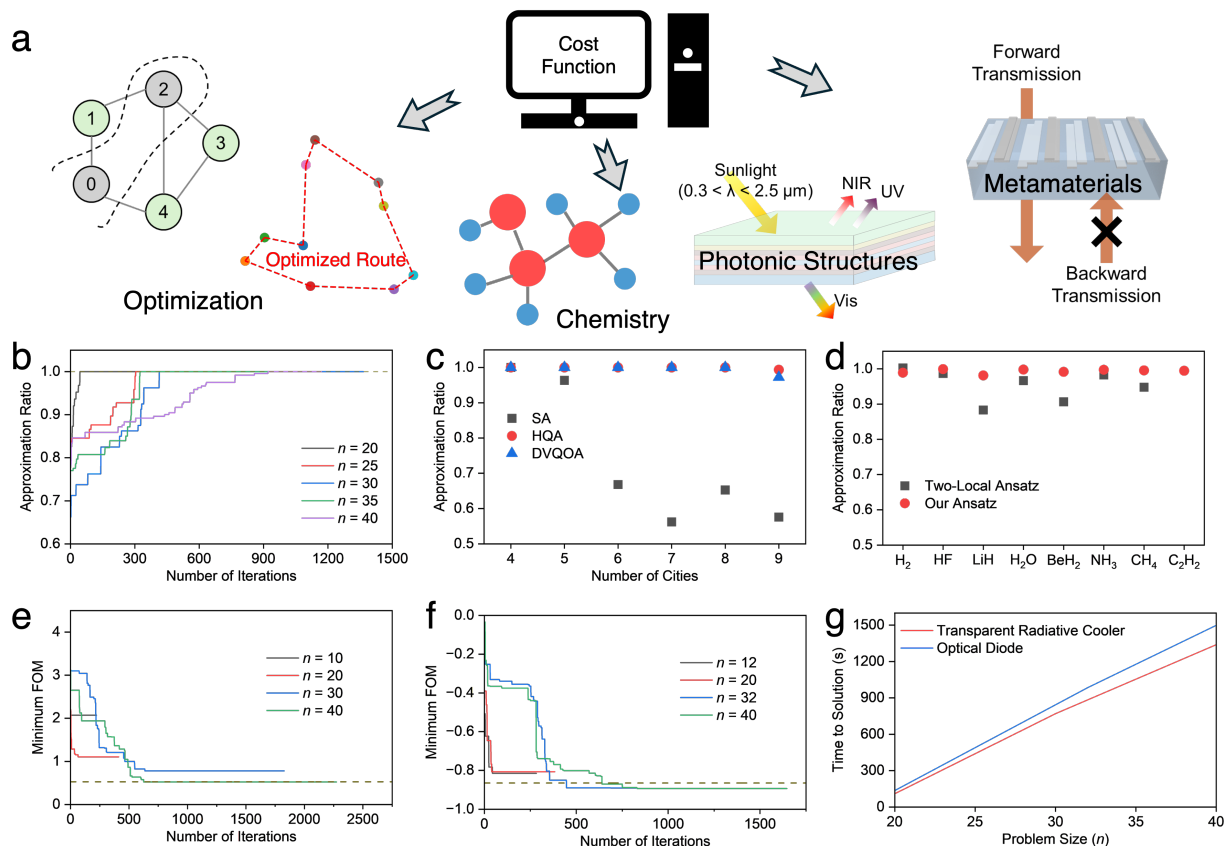


Figure 2: Applications of DVQOA to solve various problems. **a**, Schematic representation of DVQOA’s versatility, illustrating its ability to address various real-world problems by redefining the cost function. **b**, Evolution of the approximation ratio for Max-Cut problems with various n . **c**, Approximation ratio for TSP with varying number of cities to visit. **d**, Approximation ratio for computing the minimum eigenvalue of molecular Hamiltonians, highlighting DVQOA’s capability as an eigensolver. **e, f**, Evolution of FOM for real-world material optimization challenges: layered photonic structures (**e**) and metamaterial optical diodes (**f**). Dotted lines indicate the best-known results, highlighting DVQOA’s superior performance in identifying high-quality solutions. These optimization examples exhibit an exponential optimization space (2^n). **g**, Time to solution for completing material optimization tasks as a function of n , demonstrating DVQOA’s capability for completing such complex optimization tasks with a linear complexity $O(nmt)$.

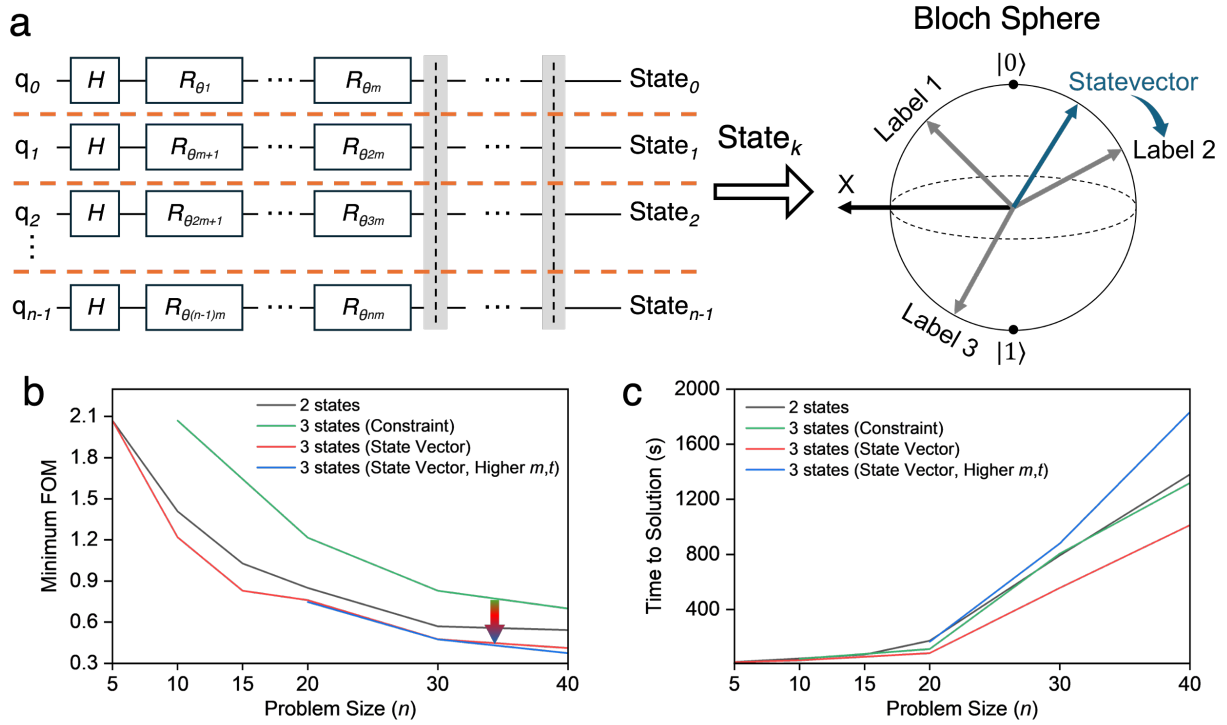


Figure 3: State vector on the Bloch sphere for N -ary optimization with DVQOA. **a**, Schematic illustrating how each state is encoded as a unique vector on the Bloch sphere, allowing a single qubit to represent one of N possible states without requiring additional qubits or constraints. **b**, Minimum FOM as a function of n for material optimization tasks. Four DVQOA methods are compared: (i) two-state encoding per qubit, (ii) three-state encoding with additional qubits and constraints, (iii) three-state encoding using a state vector on the Bloch sphere, and (iv) three-state encoding using a state vector on the Bloch sphere with increased m and t . **c**, Time to solution for completing optimization tasks as a function of n .

Table 1: Performance of DVQOA for higher-order ($k \geq 3$) binary optimization problems ($N = 2$). Approximation ratio and time to solution achieved by DVQOA and DDNN for different interaction orders (k) and problem sizes (n). Higher-order problems include all interactions of lower orders; e.g., 3^{rd} -order problems involve self-, pairwise, and three-variable interactions, significantly increasing problem complexity. Problem sizes range from 24 to 30, with instances labeled 'Pk-n'. The results demonstrate that DVQOA identifies the ground truth with substantially shorter times for complex problems, compared to brute force search and DDNN, emphasizing the practical advantage of utilizing the quantum algorithm.

k	3			4			5		
Instances	P3-26	P3-28	P3-30	P4-24	P4-26	P4-28	P5-22	P5-24	P5-26
DVQOA Approximation Ratio	1	1	1	1	1	1	1	1	1
DVQOA Time to Solution (s)	392.685	469.775	530.158	369.161	402.766	498.876	332.853	487.724	596.293
DDNN Approximation Ratio	0.9787	1	1	0.9903	1	1	1	1	1
DDNN Time to Solution (s)	328.226	398.4923	497.4745	1850.603	2573.306	3534.801	6269.772	10164.69	15549.36
Brute Force Time (s)	1,213,031	3,581,267	18,239,898	1,416,661	7,625,766	25,148,563	1,011,141	4,345,634	25,107,394
Acceleration	0.8358	0.8482	0.9383	5.0129	6.3890	7.0855	18.8364	20.8410	26.0766

Table 2: Performance of DVQOA for N -ary problems involving higher-order interactions.

Approximation ratio and time to solution of DVQOA for N -ary problems ($N = 2, 3, 4,$ and 5) involving 2^{nd} -order and 3^{rd} -order interactions, for $n = 12$. The table demonstrates that while brute force search requires exponential time to identify the ground truth, DVQOA achieves the ground truth effectively. Here, the hyperparameters (m, t) are both 3 for $N \leq 4$, and are both 7 for $N = 5$.

k	2				3			
N	2	3	4	5	2	3	4	5
Approximation Ratio	1	1	1	1	1	1	1	1
Time to Solution (s)	6.083	6.112	6.986	38.42	5.184	6.486	9.654	36.10
Brute Force Time (s)	2.281	121.7	10,739	127,990	8.639	485.5	34,134	471,200

References

1. T. D. Ladd, et al., Quantum computers. *nature* 464 (7285), 45–53 (2010).
2. D. Herr, F. Nori, S. J. Devitt, Optimization of lattice surgery is NP-hard. *npj quantum information* 3 (1), 35 (2017).
3. J. L. O’Brien, Optical quantum computing. *Science* 318 (5856), 1567–1570 (2007).
4. M. Dupont, et al., Quantum-enhanced greedy combinatorial optimization solver. *Science Advances* 9 (45), eadi0487 (2023).
5. D. P. DiVincenzo, Quantum computation. *Science* 270 (5234), 255–261 (1995).
6. L. K. Grover, Synthesis of quantum superpositions by quantum computation. *Physical review letters* 85 (6), 1334 (2000).
7. M. J. Schuetz, J. K. Brubaker, H. G. Katzgraber, Combinatorial optimization with physics-inspired graph neural networks. *Nature Machine Intelligence* 4 (4), 367–377 (2022).
8. M. Cerezo, et al., Variational quantum algorithms. *Nature Reviews Physics* 3 (9), 625–644 (2021).
9. Y. Wang, J. Liu, A comprehensive review of quantum machine learning: from NISQ to fault tolerance. *Reports on Progress in Physics* (2024).
10. F. Leymann, J. Barzen, The bitter truth about gate-based quantum algorithms in the NISQ era. *Quantum Science and Technology* 5 (4), 044007 (2020).
11. A. Abbas, et al., Challenges and opportunities in quantum optimization. *Nature Reviews Physics* pp. 1–18 (2024).
12. C. Gambella, A. Simonetto, Multiblock ADMM heuristics for mixed-binary optimization on classical and quantum computers. *IEEE Transactions on Quantum Engineering* 1, 1–22 (2020).
13. R. Shaydulin, et al., Evidence of scaling advantage for the quantum approximate optimization algorithm on a classically intractable problem. *Science Advances* 10 (22), eadm6761 (2024).
14. J. Larkin, M. Jonsson, D. Justice, G. G. Guerreschi, Evaluation of QAOA based on the approximation ratio of individual samples. *Quantum Science and Technology* 7 (4), 045014 (2022).
15. E. Pelofske, A. Bartschi, S. Eidenbenz, Short-depth QAOA circuits and quantum annealing on higher-order Ising models. *npj Quantum Information* 10 (1), 30 (2024).
16. E. Pelofske, A. Bartschi, L. Cincio, J. Golden, S. Eidenbenz, Scaling whole-chip QAOA for higher-order Ising spin glass models on heavy-hex graphs. *npj Quantum Information* 10 (1), 109

(2024).

17. W. Huang, et al., Fidelity benchmarks for two-qubit gates in silicon. *Nature* 569 (7757), 532–536 (2019).

18. T. Yamamoto, R. Ohira, Error suppression by a virtual two-qubit gate. *Journal of Applied Physics* 133 (17) (2023).

19. A. D. C´orcoles, et al., Demonstration of a quantum error detection code using a square lattice of four superconducting qubits. *Nature communications* 6 (1), 6979 (2015).

20. D. Amaro, M. Rosenkranz, N. Fitzpatrick, K. Hirano, M. Fiorentini, A case study of variational quantum algorithms for a job shop scheduling problem. *EPJ Quantum Technology* 9 (1), 5 (2022).

21. U. Azad, B. K. Behera, E. A. Ahmed, P. K. Panigrahi, A. Farouk, Solving vehicle routing problem using quantum approximate optimization algorithm. *IEEE Transactions on Intelligent Transportation Systems* 24 (7), 7564–7573 (2022).

22. M. N. Farooqi, M. Ruefenacht, Exploring Hybrid Classical-Quantum Compute Systems through Simulation, in *2023 IEEE International Conference on Quantum Computing and Engineering (QCE) (IEEE)*, vol. 2 (2023), pp. 127–133.

23. T. Beck, et al., Integrating quantum computing resources into scientific HPC ecosystems. *Future Generation Computer Systems* 161, 11–25 (2024).

24. E. Pelofske, A. Bartschi, J. Golden, S. Eidenbenz, High-Round QAOA for MAX k -SAT on Trapped Ion NISQ Devices, in *2023 IEEE International Conference on Quantum Computing and Engineering (QCE) (IEEE)*, vol. 1 (2023), pp. 506–517.

25. Q. Xu, X. Tan, D. Bao, R. Huang, Classical verification of quantum measurement for the computational basis and the XY-plane basis. *Physical Review A* 107 (5), 052616 (2023).

26. G. G. Guerreschi, J. Hogaboam, F. Baruffa, N. P. Sawaya, Intel Quantum Simulator: A cloud ready high-performance simulator of quantum circuits. *Quantum Science and Technology* 5 (3), 034007 (2020).

27. S. Efthymiou, et al., Qibo: a framework for quantum simulation with hardware acceleration. *Quantum Science and Technology* 7 (1), 015018 (2021).

28. J. R. McClean, S. Boixo, V. N. Smelyanskiy, R. Babbush, H. Neven, Barren plateaus in quantum neural network training landscapes. *Nature communications* 9 (1), 4812 (2018).

29. S. Bravyi, A. Kliesch, R. Koenig, E. Tang, Obstacles to variational quantum optimization from

- symmetry protection. *Physical review letters* 125 (26), 260505 (2020).
30. S. H. Sack, R. A. Medina, A. A. Michailidis, R. Kueng, M. Serbyn, Avoiding barren plateaus using classical shadows. *PRX Quantum* 3 (2), 020365 (2022).
 31. L. Giuffrida, D. Volpe, G. A. Cirillo, M. Zamboni, G. Turvani, Engineering Grover adaptive search: Exploring the degrees of freedom for efficient QUBO solving. *IEEE Journal on Emerging and Selected Topics in Circuits and Systems* 12 (3), 614–623 (2022).
 32. G. Turati, M. F. Dacrema, P. Cremonesi, Feature selection for classification with QAOA, in 2022 IEEE International Conference on Quantum Computing and Engineering (QCE) (IEEE) (2022), pp. 782–785.
 33. S. Kim, T. Luo, E. Lee, I.-S. Suh, Distributed Quantum Approximate Optimization Algorithm on Integrated High-Performance Computing and Quantum Computing Systems for Large-Scale Optimization. arXiv preprint arXiv:2407.20212 (2024).
 34. C. W. Commander, Maximum cut problem, MAX-cut. *Encyclopedia of Optimization* 2 (2009).
 35. U. Benlic, J.-K. Hao, Breakout local search for the max-cut problem. *Engineering Applications of Artificial Intelligence* 26 (3), 1162–1173 (2013).
 36. G. A. Kochenberger, J.-K. Hao, Z. Liu, H. Wang, F. Glover, Solving large scale max cut problems via tabu search. *Journal of Heuristics* 19, 565–571 (2013).
 37. Q. Xu, K. Setia, Truncation technique for variational quantum eigensolver for Molecular Hamiltonians. arXiv preprint arXiv:2402.01630 (2024).
 38. Q. H. Tran, S. Kikuchi, H. Oshima, Variational denoising for variational quantum eigensolver. *Physical Review Research* 6 (2), 023181 (2024).
 39. M. Kim, et al., Visibly transparent radiative cooler under direct sunlight. *Advanced Optical Materials* 9 (13), 2002226 (2021).
 40. S. Kim, et al., High-performance transparent radiative cooler designed by quantum computing. *ACS Energy Letters* 7 (12), 4134–4141 (2022).
 41. S. So, et al., Radiative cooling for energy sustainability: from fundamentals to fabrication methods toward commercialization. *Advanced Science* 11 (2), 2305067 (2024).
 42. S. Kim, et al., Quantum annealing-aided design of an ultrathin-metamaterial optical diode. *Nano Convergence* 11 (1), 16 (2024).
 43. Z. Xu, et al., Quantum-inspired genetic algorithm for designing planar multilayer photonic

- structure. *npj Computational Materials* 10 (1), 257 (2024).
44. K. Kitai, et al., Designing metamaterials with quantum annealing and factorization machines. *Physical Review Research* 2 (1), 013319 (2020).
45. T. Lookman, P. V. Balachandran, D. Xue, R. Yuan, Active learning in materials science with emphasis on adaptive sampling using uncertainties for targeted design. *npj Computational Materials* 5 (1), 21 (2019).
46. K. M. Jablonka, G. M. Jothiappan, S. Wang, B. Smit, B. Yoo, Bias free multiobjective active learning for materials design and discovery. *Nature communications* 12 (1), 2312 (2021).
47. S. Kim, et al., A review on machine learning-guided design of energy materials. *Progress in Energy* (2024).
48. N. Herrmann, et al., First quantum machine learning applications on an on-site room-temperature quantum computer. *arXiv preprint arXiv:2312.11673* (2023).

Acknowledgments

We thank Nils Herrmann and John L. Helm from Quantum Brilliance, and Vincent R. Pascuzzi from IBM for their insightful discussion.

Funding: This research used resources of the Oak Ridge Leadership Computing Facility at the Oak Ridge National Laboratory, which is supported by the Office of Science of the U.S. Department of Energy under Contract No. DE-AC05-00OR22725. This material is based upon work supported by the U.S. Department of Energy, Office of Science, National Quantum Information Science Research Centers, Quantum Science Center.

Notice: This manuscript has in part been authored by UT-Battelle, LLC under Contract No. DE-AC05-00OR22725 with the U.S. Department of Energy. The United States Government retains and the publisher, by accepting the article for publication, acknowledges that the U.S. Government retains a non-exclusive, paid up, irrevocable, world-wide license to publish or reproduce the published form of the manuscript, or allow others to do so, for U.S. Government 15 purposes. The Department of Energy will provide public access to these results of federally sponsored research in accordance with the DOE Public Access Plan (<http://energy.gov/downloads/doe-publicaccess-plan>).

Author contributions: Conceptualization, methodology, investigation, data collection, data analysis and visualization: S.K.; Expertise: S.K., and I.S.; Funding acquisition: S.K., and I.S.; Writing: S.K., and I.S.

Competing interests: The authors declare no competing interests.

Data and materials availability: All data are available in the manuscript or the supplementary materials. Information requests are available from the corresponding author upon reasonable request.

Supplementary materials

Materials and Methods

Supplementary Text

Figs. S1 to S14

Tables S1 to S5

References (49-60)

Supplementary Materials for Distributed Variational Quantum Algorithm with Many-qubit for Optimization Challenges

Seongmin Kim and In-Saeng Suh

National Center for Computational Sciences, Oak Ridge National Laboratory, Oak Ridge, Tennessee
37830, United States.

Corresponding author. Email: kims@ornl.gov, suhi@ornl.gov

This PDF file includes:

Materials and Methods

Supplementary Text

Figures S1 to S14

Tables S1 to S5

References

Materials and Methods

Computational experiments

We use qiskit (version 0.41.0) for developing and executing the quantum algorithm, while the newer version (1.2.4) is employed for the execution of the quantum algorithm on quantum hardware. For quantum simulation, we utilize qiskit-aer (version 0.11.2) with the 'automatic' or 'statevector' method. For classical optimization, we employ the 'scipy.optimize.minimize' (SciPy version 1.2.1) with a gradient-free optimizer 'COBYLA' to minimize the cost function. Parameters in rotation gates in our ansatz are randomly initialized within the range $[-2\pi, 2\pi]$, and these parameters are iteratively adjusted through classical optimization.

To implement our quantum algorithm on quantum hardware and compare its performance with the simulator, the maximum number of iterations was set to 200, considering hardware access limitations and ensuring practical execution times. The hyperparameters (number of layers m and repeats t) are set to 3, and the number of partitions is set to 1 for this analysis. Specifically, we utilize the IBM-Nazca and IBM-Strasbourg quantum devices, which feature 127 qubits, to evaluate and validate the algorithm's performance on real quantum computing devices. For this study, a MacBook Pro, equipped with an Apple M2 Max processor and 32 GB of memory, is employed for submitting quantum circuits and processing the classical components of the algorithm without leveraging distributed execution.

Despite the observed advantage on quantum hardware, quantum simulators are used for most studies due to limited access to quantum devices. To maintain the efficiency of our quantum algorithm on the simulator, circuit widths are capped at 10 qubits (Fig. S2). The optimization process terminates upon achieving full convergence (by default tolerance) or reaching a predefined maximum iteration limit (5,000 in this study). For small-scale problems, convergence is usually achieved before reaching the maximum iterations. However, for large-scale problems ($n \geq 100$), convergence tends to be less stable, leading to unnecessarily extended optimization runs, thus increasing computational costs. To address this issue, an additional stopping criterion is introduced: if the cost value changes by less than 0.05% over the 500 consecutive iterations, the optimization process is terminated. This dual-criterion approach ensures computational efficiency while maintaining accuracy across diverse problem scales. For scalability studies, 100- to 1,000-qubit Max-Cut problems

with five different instances are addressed without distributed execution using the MacBook Pro. In addition, hyperparameters (m and t) are set to 3.

Integrating high-performance computing (HPC) with quantum computing (QC)

Two HPC systems are utilized for the integration with QC: “Frontier” and “Defiant”, both located at the Oak Ridge Leadership Computing Facility. While these systems feature similar hardware and software architectures, Frontier offers more compute nodes, enabling superior scalability for large-scale computations. Each compute node in Defiant is equipped with 64-core AMD EPYC 7662 “Rome” CPUs and 256 GB of memory. Frontier nodes, on the other hand, feature 64-core AMD “Optimized 3rd Gen EPYC” CPUs and provide 512 GB of memory per node.

For efficient task allocation, Defiant is employed for smaller problems requiring fewer than 30 compute nodes (1,500 CPU cores), benefiting from shorter queue times. Conversely, Frontier is reserved for larger problems that demand over 1,500 CPU cores (30 compute nodes), leveraging its extensive computational resources for scalability. All distributed computations, including the execution of distributed variational quantum optimization algorithm (DVQOA), distributed deep neural network (DDNN), and brute-force searches, are performed using a message-passing interface (MPI) implementation.

Quadratic unconstrained binary optimization (QUBO) problems

QUBOs model the energy function of a certain system (49), and real-world problems are generally represented as fully connected QUBOs (33), where all variables interact with one another. To simulate such complex real-world scenarios, QUBO instances used in this study are constructed as fully connected matrices with random elements uniformly distributed between -1 and 1. The energy of the QUBO serves as a cost function for optimization.

Brute force search guarantees the identification of the ground truth for QUBO problems (31), with an exponential complexity of $O(2^n)$. For problem size $n < 40$, the ground truths are determined by brute force search with HPC systems, leveraging up to 8,192 CPU cores (164 compute nodes). These solutions serve as references for calculating the approximation ratio, which is defined as: Approximation Ratio = (Identified Value / Ground Truth). The total brute force computation time is estimated by multiplying the runtime of an MPI task with the number of cores employed, i.e.,

Brute Force Time = MPI Task Runtime \times Number of Cores. This represents the total time required if brute force is performed on a single core. The generated QUBO instances are further utilized for hyperparameter studies, exploring the effects of hyperparameters (m and t).

Max-Cut problems

Max-Cut problems are a fundamental class of binary combinatorial optimization problems, where each variable can take binary values (0 or 1), and the objective considers self- and pairwise interactions between variables (34). As the number of nodes (n) increases, the potential number of edges grows significantly, with a maximum of $n(n-1)/2$. To adjust problem complexity, the sparsity of Max-Cut instances can be controlled by varying the number of edges. For this study, we generate relatively dense configurations with the number of edges set to $n(n-1)/8$.

Numerous classical and quantum solvers have been developed to solve Max-Cut problems, with hybrid quantum annealing (HQA; D-Wave Systems, Advantage system 4.1) recognized as one of the most effective solvers (50). As demonstrated in Table S1, HQA achieves solutions close to or slightly better than the best-known values, though occasional suboptimal results are also observed (7, 35, 36). Brute force search, while guaranteeing exact solutions, becomes infeasible for large problem sizes ($n > 40$) due to its exponential time complexity. Consequently, for such large Max-Cut problems, the solutions obtained from HQA are used as reference values to calculate the approximation ratio, defined as: Approximation Ratio = (Identified Value / Reference Value). This approach ensures a reliable evaluation of algorithm performance across both moderate and large-scale Max-Cut problem instances. As Max-Cut problems can be formulated as QUBO problems, the QUBO energy serves as the cost function for optimization.

Traveling salesman problems

The traveling salesman problem (TSP) is another example of a combinatorial optimization problem where quantum computing has the potential to exhibit a clear advantage. TSP is classically challenging due to the factorial growth of possible routes ($n!$), where n is the number of cities to visit. In our experiments, cities are randomly distributed within the range $[0,10]$, and the objective is to minimize the total travel distance required to visit every city exactly once. To encode these problems as QUBOs not to visit the same cities, penalty factors are applied with a value of 100. The

ground truth for the cost function, representing the shortest path, is determined using brute-force search.

DVQOA is employed to solve the QUBOs that represent the TSP, with the obtained solutions converted into city indices representing the optimal order of cities to visit. Simulated annealing (SA), a classical solver that search optimization spaces by modeling thermal fluctuation, is used to solve the TSP, but it usually fails to find the optimal routes. HQA, recognized as one of the best solvers for QUBO-type problems as demonstrated in Max-Cut problems, is also applied to the TSP. Solution quality is evaluated using the approximation ratio, defined as Approximation Ratio = $(\text{Cost}_{\text{global}} / \text{Cost}_{\text{solver}})$. By definition, an approximation ratio close to 1 indicates a high-quality solution.

Hyperparameters in DVQOA are adjusted to solve more complex problems: m and t are set to 3 for problems with fewer than 7 cities, and 7 for problems with 7 and 9 cities.

Chemistry problems

Quantum-classical algorithms have been widely explored for quantum chemistry calculations, particularly for determining the lowest energy states of molecules. Since the computational cost scales exponentially with a system size, variational quantum eigensolvers (VQEs) have gained significant attention as a promising approach leveraging quantum principles (37, 38).

In this study, we select eight molecules—Hydrogen (H_2), Hydrogen Fluoride (HF), Lithium Hydride (LiH), Hydrogen Dioxide (H_2O_2), Beryllium Hydride (BeH_2), Ammonia (NH_3), Methane (CH_4), and Acetylene (C_2H_2)—to compute their ground-state energies. The molecular Hamiltonian is mapped onto a qubit operator to construct the cost Hamiltonian using `qiskit-nature` and `pyscf`. A two-local ansatz, composed of Ry gates and CNOT gates, is employed for energy estimation using VQE, implemented in `qiskit-algorithms`. The COBYLA optimizer is used for classical optimization, with a maximum of 500 iterations. Parameters are initialized within the range $[-2\pi, 2\pi]$, and energy values are estimated using a noiseless simulator (`AerEstimator`). VQE is executed in a distributed computing environment with 500 cores across 10 compute nodes.

Our DVQOA efficiently calculates eigenvalues for quantum chemistry problems using a state-vector estimator, eliminating the need for computational state measurements. This approach allows the eigenvalues to be determined directly from circuit parameters and the cost Hamiltonian. The

lowest molecular energy (ground state) is obtained using the 'NumPyMinimumEigensolver' on a classical computer, serving as a reference for computing the approximation ratio: Approximation Ratio = (Energy_{solver} / Ground State).

Layered photonic structures

Layered photonic structures serve as a practical testbed to show the efficiency of DVQOA in solving complex optimization problems within material science. These structures can have unique optical characteristics, such as transmitting visible photons while reflecting ultraviolet (UV) and near-infrared (NIR) photons, making them suitable for optical filter applications like energy-saving windows (40, 43, 51). Furthermore, by incorporating a thermal radiative layer on the top surface, such photonic structures can have radiative cooling performance by emitting thermal radiation through an atmospheric window ($8 \mu\text{m} < \lambda < 13 \mu\text{m}$) to mitigate the global warming issue (52). Hence, these structures can be employed for developing transparent radiative coolers (39, 40, 51).

Fig. S12 illustrates the design involves a silica substrate with a top layer of 40 μm -thick polydimethylsiloxane (PDMS), and the thickness of the photonic structure is set to 1.2 μm . Each layer in the photonic structures can be one of four materials: silicon dioxide (SiO_2), silicon nitride (Si_3N_4), aluminum oxide (Al_2O_3), and titanium dioxide (TiO_2). They can be encoded with two-digit binary labels: '00' for SiO_2 , '01' for Si_3N_4 , '10' for Al_2O_3 , and '11' for TiO_2 . Hence, a 6-layered photonic structure corresponds to a bitstring length of 12 (i.e., problem size or circuit width $n = 12$). Photons can be transmitted or reflected depending on the refractive contrast at the interface between layers, thus optimizing layer configuration is important to achieve desirable optical characteristics. However, exponentially large design space arising from 2^n possible configurations makes it challenging to solve these optimization problems.

Energy-saving windows aim to maximize transmitted irradiance in the visible range while minimizing it in the UV/NIR ranges (39, 40). An ideal design achieves perfect transmission efficiency in the visible range, and zero transmission in other ranges (Fig. S14). To evaluate the performance of a designed photonic structure, a figure-of-merit (FOM) is introduced (40, 51):

$$TI(\lambda) = T(\lambda) \times S(\lambda), \quad (\text{S1})$$

$$\text{FOM} = \frac{10 \int_{300}^{2500} (TI_{\text{designed}}(\lambda) - TI_{\text{ideal}}(\lambda))^2 d\lambda}{\int_{300}^{2500} S(\lambda)^2 d\lambda}, \quad (\text{S2})$$

where $T(\lambda)$ and $S(\lambda)$ respectively represent transmission efficiency and the solar spectral irradiance (under air mass 1.5 global (53)). Here, transmission efficiency $T(\lambda)$ is calculated with the transfer matrix method, a computationally efficient methodology for layered structures (54). $TI(\lambda)$ is the transmitted irradiance through the designed or ideal photonic structures. By definition, a lower FOM indicates that the optical properties of the designed structure closely match those of the ideal structure, indicating a superior design. Consequently, this problem aligns well with the minimization capabilities of DVQOA, which effectively uses FOM as the cost function, making it an effective algorithm for addressing such complex material design challenges.

Metamaterial optical diodes

Optical diodes are essential components in photonics, designed to allow unidirectional light transmission while blocking light in the reverse direction (42, 55, 56). They are crucial for protecting optical sources and processing optical information efficiently (42). Thin optical diode designs often leverage pixelated metamaterials, where each pixel is assigned as either dielectric ('0') or metallic ('1') materials (Fig. S13). These metamaterial optical diodes should achieve high forward transmission (T_F) and low (near-zero) backward transmission (T_B) to exhibit effective unidirectional optical behavior.

Asymmetric transmission is realized by enabling first-order diffraction only for forward incident light. This behavior is achieved when the following condition is satisfied:

$$\frac{2n_1\pi}{\lambda_0} < \frac{2\pi}{\Lambda_G} < \frac{2n_2\pi}{\lambda_0}, \quad (\text{S3})$$

where n_1 and n_2 are the refractive indices of the upper and lower media, respectively. Λ_G represents the periodic length of the unit cell, and λ_0 denotes the wavelength of the incident light. In this study, we set the parameters n_1 , n_2 , Λ_G , and λ_0 to 1 (air), 1.45 (silicon dioxide), 600 nm, and 800 nm, respectively. Under these conditions, we optimize pixel configurations within the unit cell of a metamaterial optical diode to achieve the desired unidirectional optical behavior.

To evaluate the performance of a designed optical diode, FOM is defined as: $FOM = T_B - T_F$. Here, transmission efficiency is calculated using rigorous coupled wave analysis, which is a semi-analytical method for solving Maxwell's equation (57). The optimization of pixelated metamaterial configurations is important to achieve the desired optical diode performance, characterized by a low FOM. However, the optimization space grows exponentially (2^n possible configurations), with the number of pixels n , making this problem computationally challenging. Our DVQOA is particularly well-suited for addressing this type of minimization problem (with FOM as the cost function), offering a promising approach for exploring the large material optimization space efficiently to identify the optimal structure.

Distributed deep neural networks

Deep neural networks (DNNs) are well-suited for binary optimization tasks, leveraging the sigmoid activation function to output probabilities associated with binary values for each variable. Our DNN architecture consists of two hidden layers with 128 and 64 neurons, respectively. The Adam optimizer is employed with a learning rate of 0.001, and the network is trained over 500 epochs to minimize the cost function. Input data is initialized within the range $[0,1]$. The cost function corresponds to the energy state of a given problem, enabling the DNN to identify a binary vector that minimizes the cost function of the optimization problem.

To improve performance, the distributed execution of DNNs (DDNN) across multiple cores and nodes is implemented using MPI. By utilizing 500 cores distributed across 10 compute nodes, similar to our distributed quantum approach (DVQOA), DDNN enhances the chance of identifying the ground truth solution through diverse parameter configurations. Among the solutions generated by DDNN, the best solution is selected to calculate the approximation ratio. The time to solution is measured from the task initiation to its completion.

Supplementary Text

Variational principle

Variational quantum algorithms (VQAs) leverage the variational principle of quantum mechanics to approximate the ground state eigenvalue (λ_0) of a Hamiltonian H (8, 58). This is achieved by evaluating the expectation value of H with a variational state $|\psi_k\rangle$, as the following equations:

$$\lambda_{n-1} > \lambda_k > \dots > \lambda_0 \quad (\text{ground state}), \quad (\text{S4})$$

$$H = \sum_{t=0}^{n-1} \lambda_t |\lambda_t\rangle\langle\lambda_t|. \quad (\text{S5})$$

Here, the expectation value $\langle\psi_k|H|\psi_k\rangle$ can be written as:

$$\langle\psi_k|H|\psi_k\rangle = \langle\psi_k| \left(\sum_{t=0}^{n-1} \lambda_t |\lambda_t\rangle\langle\lambda_t| \right) |\psi_k\rangle, \quad (\text{S6})$$

$$\langle\psi_k|H|\psi_k\rangle \geq \sum_{t=0}^{n-1} \lambda_0 \langle\psi_k|\lambda_t\rangle\langle\lambda_t|\psi_k\rangle, \quad (\text{S7})$$

$$\sum_{t=0}^{n-1} \lambda_0 \langle\psi_k|\lambda_t\rangle\langle\lambda_t|\psi_k\rangle = \lambda_0, \quad (\text{S8})$$

$$\langle\psi_k|H|\psi_k\rangle \geq \lambda_0. \quad (\text{S9})$$

According to the Variational principle, a parameterized quantum circuit generates a variational state $|\psi_k(\vec{\theta})\rangle$, where $\vec{\theta}$ denotes the trainable parameters of the quantum gates. By optimizing these parameters, the algorithm converges to the optimal state that yields the closest approximation to the ground state.

Execution of DVQOA on quantum hardware and simulator

Approximation ratios in this analysis may appear relatively low due to the constrained number of iterations and the lack of hyperparameter optimization. Nevertheless, as can be seen in Fig. 1b, both the quantum hardware and simulator achieve satisfactory approximation ratios (> 0.9 for n

≤ 30). This result is particularly notable as the quantum algorithm executed on hardware achieves approximation ratios nearly as high as those obtained on the simulator, despite the presence of hardware noise. This observation highlights the robustness of VQOA against errors introduced by hardware imperfections.

Despite achieving comparable approximation ratios on a real quantum device and quantum simulator, they exhibit fundamentally different scaling behaviors for executing quantum circuits. Quantum hardware inherently leverages the superposition states of qubits within the quantum processing unit (QPU), making circuit width independent of hardware runtime (59). As illustrated in Fig. 1c, this results in a constant execution time for the algorithm on a real quantum device, even as circuit width (i.e., problem size, n) increases. For this analysis, the time to solution is measured by excluding the queue time for quantum device access from the total runtime of quantum-classical hybrid computations. This ensures that the evaluation focuses exclusively on the algorithm’s intrinsic execution performance (QPU usage time and classical optimization time).

In contrast, the quantum simulator experiences significantly longer execution times for large-scale problems when executing entire quantum circuits at once, as shown in Fig. 1c. Notably, the quantum simulator cannot directly handle quantum circuits with a width of 40. This limitation arises because quantum simulators running on classical computers must store all possible quantum states, requiring memory that scales exponentially with circuit width (n), and performing quantum operations accordingly (26, 27). As a result, the exponential memory demand leads to a substantial increase in simulation time as n grows (Fig. 1c). Our ansatz effectively mitigates this challenge by partitioning circuits into multiple segments, enabling large-scale quantum simulations and allowing single-qubit simulations to be performed efficiently. However, quantum simulation still scales at least linearly, highlighting the potential advantage of quantum hardware for solving large-scale problems.

Optimization problems involving higher-order interactions

Many real-world problems involve higher-order interactions among variables, not just self- or pairwise interactions (60). To evaluate the capability of DVQOA in handling such complex scenarios, problem instances are generated with coefficients representing higher-order interactions. These coefficients, randomly distributed within the range $[-1, 1]$, represent arbitrary-order interactions.

For instance, optimization problems considering 3^{rd} -order interactions include 1^{st} -order (self), 2^{nd} -order (pairwise), and 3^{rd} -order (three variable) interactions. The total number of interaction coefficients grows rapidly with both the number of variables n and the interaction order k , following the formula:

$$T(n, k) = \sum_{r=1}^k \binom{n}{r} = \sum_{r=1}^k \frac{n!}{r!(n-r)!}. \quad (\text{S10})$$

The rapid growth in the number of coefficients significantly increases problem complexity. For example, $T(10,2) = 55$ when $n = 10$ and $k = 2$, whereas it rises to $T(10,3) = 175$ when $n = 10$ and $k = 3$. As k increases, the polynomial increase in problem complexity, characterized by $O(n^k)$, poses significant challenges for classical optimization approaches, making them computationally impractical for higher-order problems.

Comparison between DVQOA and DDNN for challenging problems

For highly complex problems (P5-28, P5-30, P5-33, and P5-36), the extensive computational demands of the DDNN make the 50-core setup per compute node infeasible. This limitation arises from the large number of trainable parameters, which impose significant memory and computational overhead, leading to inefficient resource utilization at larger scales. To address this, we allocate computing resources as follows: 20 cores per compute node for 'P5-28 and P5-30', 15 cores per compute node for 'P5-33', and 10 cores per compute node for 'P5-36'.

In contrast, DVQOA's lightweight architecture, with the manageable number of trainable parameters, enables the full utilization of the 50-core setup per node, maintaining both high computational efficiency and accuracy. This design allows DVQOA to scale effectively even for complex optimization tasks, demonstrating its robustness and adaptability in distributed execution environments. For this study, we use 10 compute nodes for both DVQOA and DDNN, ensuring efficient parallel execution and optimal performance across large-scale problems.

The comparative results highlight a key distinction: while the DDNN struggles to efficiently utilize distributed resources for computationally demanding problems, DVQOA operates well under the same conditions, delivering scalable performance and high solution quality. Notably, although the DDNN shows scalability for simpler optimization problems, its performance deteriorates when

addressing more complex scenarios, such as those involving higher-order interactions. On the other hand, DVQOA consistently shows higher solution quality with linear scaling, even for such challenging problems, highlighting its superior performance over classical algorithms. By achieving high accuracy and significantly reduced time complexity, DVQOA effectively demonstrates the practical advantage of utilizing the quantum-classical approach in solving computationally challenging optimization tasks (Table 1 and Table S3).

***N*-ary optimization problems**

The problem complexity increases exponentially when moving from binary to *N*-ary ($N \geq 3$) optimization, where variables can assume *N* possible states rather than binary state (just 0 or 1). This transition exponentially enlarges the solution space, scaling as N^n . For example, binary problems ($N = 2$) with $n = 10$ has a solution space size of 2^{10} (= 1,024) while ternary and quaternary problems respectively have 3^{10} (= 59,049) and 4^{10} (= 1,048,576). This exponential growth in the size of the solution space with larger *N*, combined with the polynomial increase in the number of interaction coefficients, results in a problem complexity of $O(N^n n^k)$ for *N*-ary k^{th} -order optimization problems. Although brute force search ensures the identification of the ground truth, it is impractical for large values of *n*, *k*, or *N*, as the computational resources required scale prohibitively with the problem size.

State vector on the Bloch sphere for *N*-ary problems

DVQOA addresses *N*-ary optimization challenges with remarkable efficiency by leveraging state vectors on the Bloch sphere to represent multiple states for *N*-ary optimization (48). Each state is encoded as a unique vector on the Bloch sphere, allowing a single qubit to represent one of *N* possible states without requiring additional qubits or constraints (Fig. 3a). For example, with $N = 3$,

label₀: [complex(1, 0), complex(0, 0)]

label₁: [complex(-cos($\pi/3$), 0), complex(-sin($\pi/3$), 0)]

label₂: [complex(-cos($\pi/3$), 0), complex(sin($\pi/3$), 0)]

This state assignment minimizes resource requirements and computational overhead, enabling DVQOA to map state vectors to specific labels by measuring distances between the states and labels. With this approach, DVQOA achieves an approximation ratio of 1 for N -ary problems even involving higher-order interactions, highlighting its capability to accurately solve significantly complex problems.

Alternatively, additional qubits with constraints can be used to represent N -ary states (e.g., '00' for label₀, '01' for label₁, '10' and '11' for label₂ for ternary problems using two qubits). However, this method introduces additional complexity and expands the solution space, making it inefficient to identify high-quality solutions. In contrast, state vector representation on the Bloch sphere simplifies the encoding process, avoiding the need for extra qubits or constraints (Fig. 3a). This approach establishes DVQOA as a powerful tool for challenging optimization tasks involving complex variable interactions and multi-state systems.

Supplementary Figures

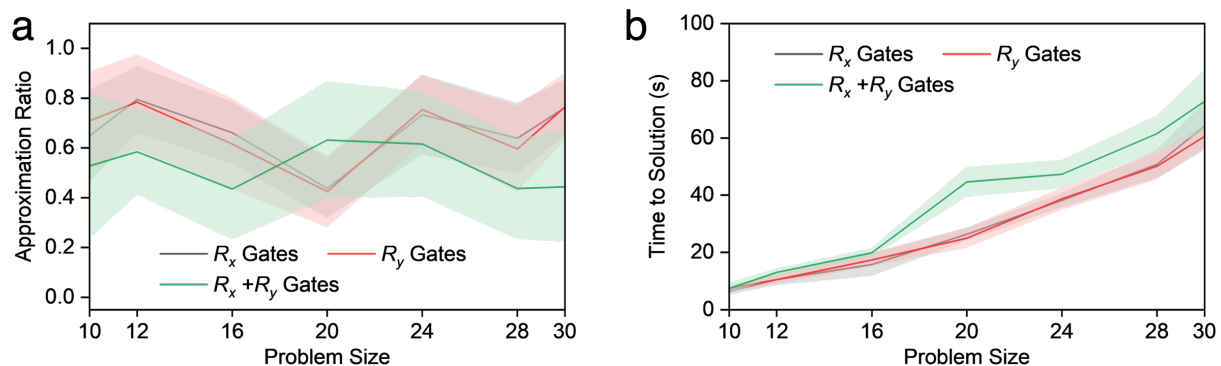


Figure S1: Investigation of efficient rotation gates for ansatz. Approximation ratio (a) and time to solution (b) when using R_x , R_y , and $R_x + R_y$ gates in the ansatz. Note that R_z gates do not affect the measured state of qubits, making R_x and R_y the effective gates for optimization. While we choose R_y gates in the circuit, selecting R_x does not affect the results.

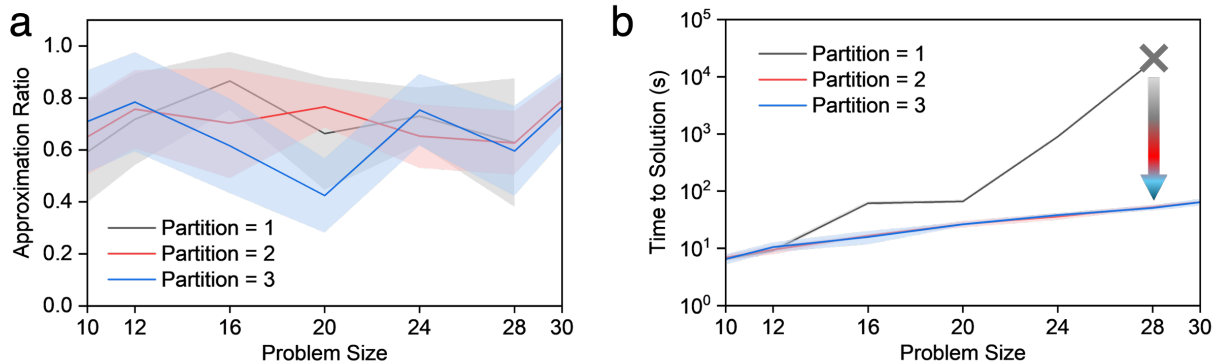


Figure S2: Partitioning capability of the designed ansatz. Approximation ratio (a) and time to solution (b) with different number of partitions. Since our ansatz does not use entangling gates, a large circuit can be segmented into multiple pieces without losing quantum information or correlations. The relationship between variables is learned through parameter optimization. Time to solution increases significantly with larger n due to quantum simulation on a classical computer, making problems with $n = 30$ challenging. This limitation can be easily mitigated by partitioning the circuit, which does not affect solution quality.

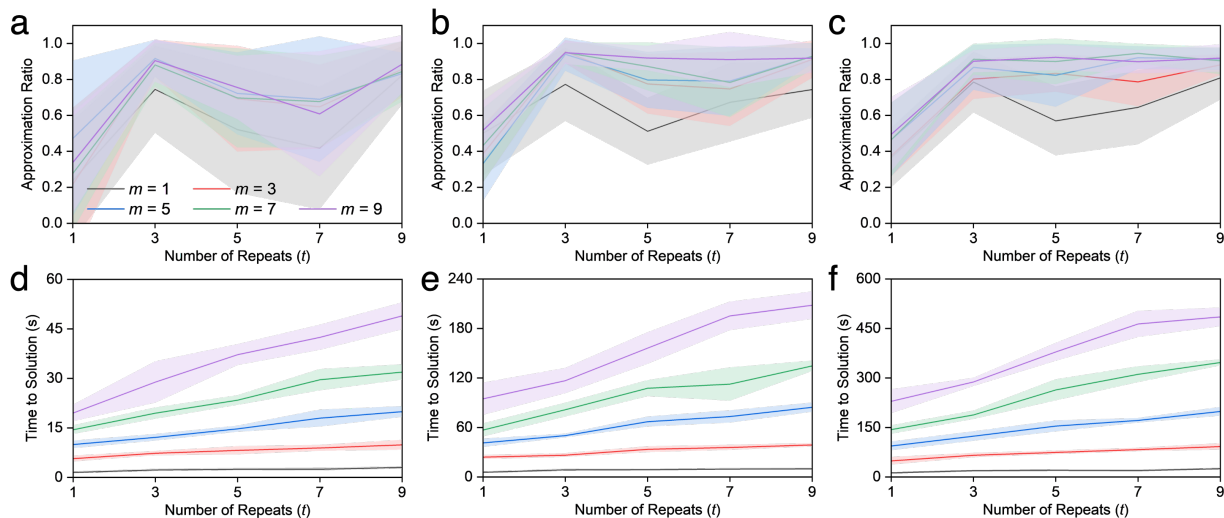


Figure S3: Hyperparameter study: the number of layers m and repeats t . Approximation ratio (a,b,c) and time to solution (d,e,f) with different hyperparameters. For this study, $n = 10$ (a,d), $n = 20$ (b,e), and $n = 30$ (c,f). For smaller problems ($n \leq 20$), smaller hyperparameter values yield better results due to manageable numbers of trainable parameters. By implementing repeated gates while keeping the number of trainable parameters smaller, the algorithm can express complex solution spaces and avoid excessive optimization effort, resulting in high performance. Furthermore, by eliminating entangling gates while enabling parameters naturally to learn complex correlation, the Barren Plateaus problem is effectively mitigated, leading to high approximation ratios.

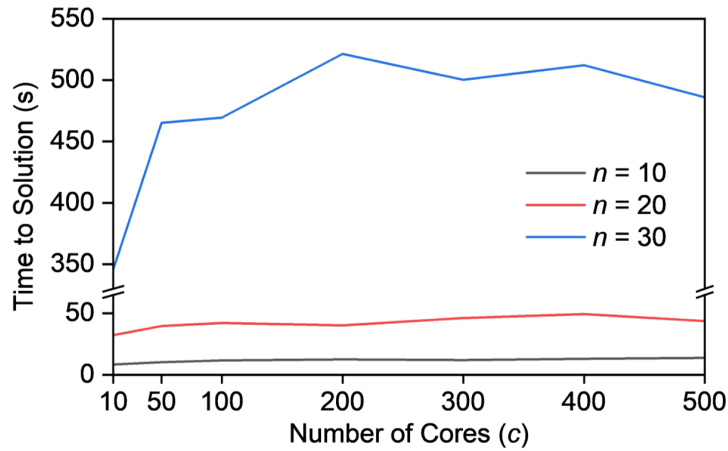


Figure S4: Distributed execution of VQOA (DVQOA) on HPC-QC integrated systems. Time to solution for different problem sizes with varying number of cores used. Note that approximation ratios are all 1 within this study. We use 50 cores per compute node, meaning 500 cores require 10 compute nodes. For $n = 30$, the time to solution is 485.95 s using 500 cores while it is 345.79 s using 10 cores (only ~41 % increase in time). Hence, to maximize the solution quality, 500 cores are used for DVQOA in further study.

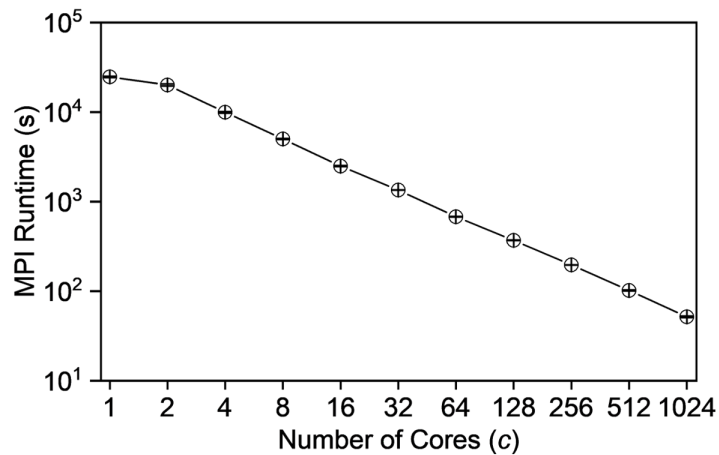


Figure S5: MPI task runtime for brute force search utilizing multiple cores (c) on the HPC system for $n = 30$. Increasing the number of cores linearly decreases the runtime with a complexity of $O(2^n/c)$.

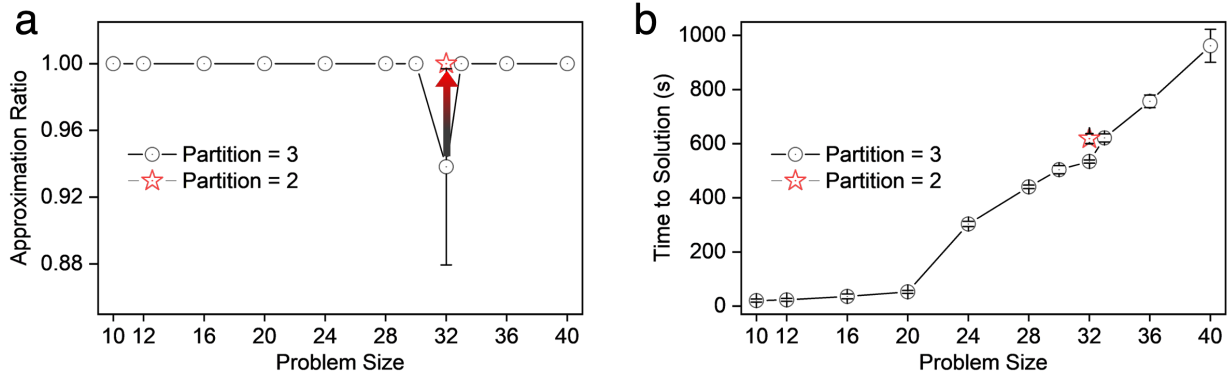


Figure S6: Impact of partitioning on the algorithm's performance. Approximation ratio (a) and time to solution (b) of DVQOA with the different number of partitions for varying problem sizes. Note that the exact solutions can be achieved when the number of partitions exactly segments an original circuit.

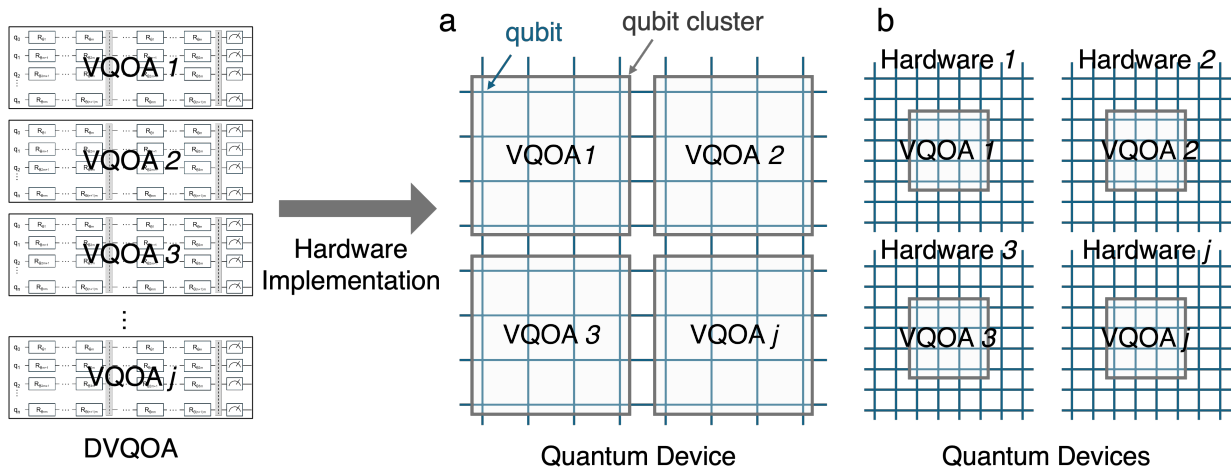


Figure S7: DVQOA on quantum hardware. a, Distributed execution of VQOAs on a single quantum device utilizing qubit clusters, with each cluster running an individual VQOA. b, Distributed execution across multiple quantum devices, with each device handling one VQOA. In both setups, the final optimization result is determined by selecting the best solution from all executed VQOAs, following the approach used in DVQOA on quantum simulators.

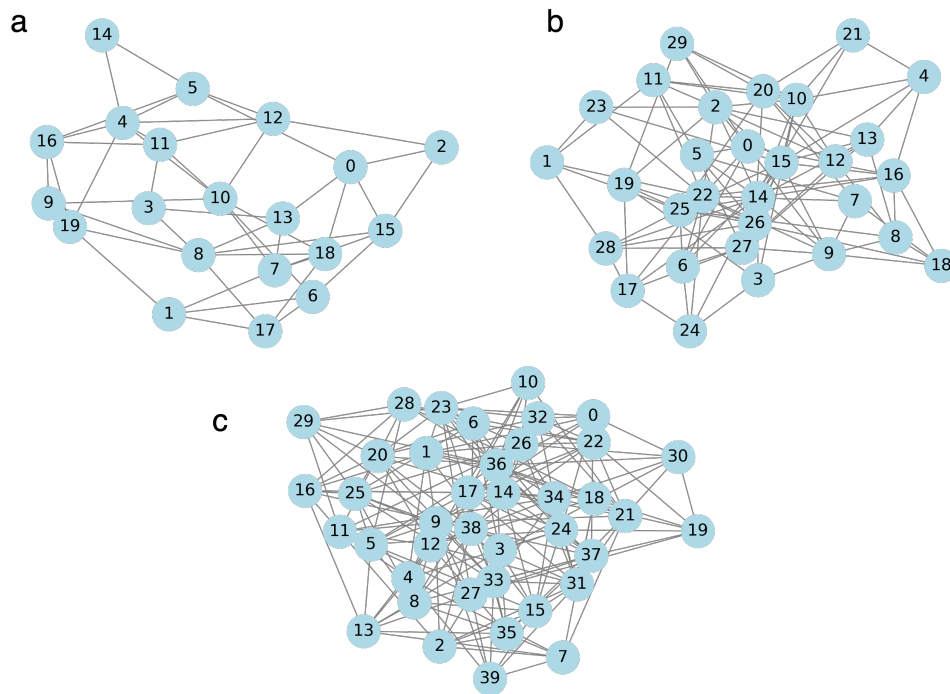


Figure S8: Max-Cut problems. Schematic representation of Max-Cut problems with different problem sizes (number of nodes n). $n = 10$ (a), $n = 20$ (b), and $n = 30$ (c). The number of edges for each problem instance is set to $n(n-1)/8$.

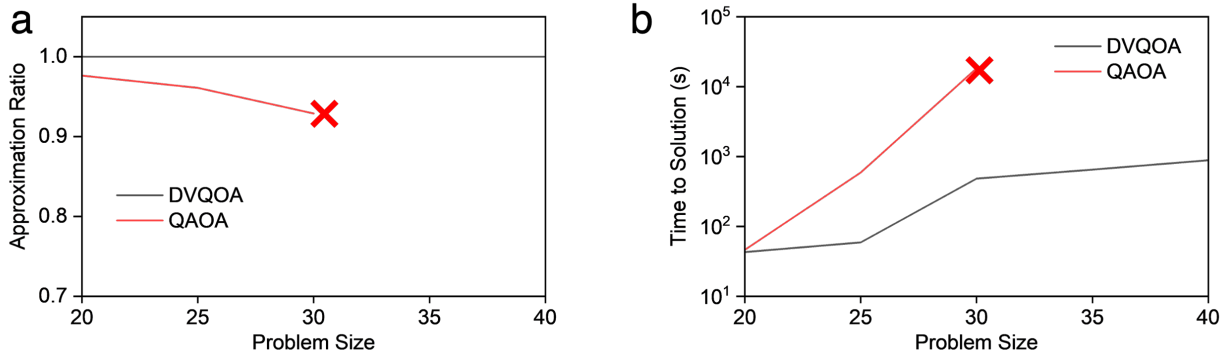


Figure S9: Performance comparison between DVQOA and QAOA for Max-Cut problems. Approximation ratio (a) and time to solution (b) as a function of n . As observed in QUBO problems, QAOA shows degraded performance for Max-Cut problems as n increases, while DVQOA maintains stable performance across varying sizes. Notably, QAOA cannot solve problems with $n > 30$ due to excessive computational efforts required. The red cross denotes that QAOA fails to solve problems larger than 30 nodes due to excessive circuit depth.

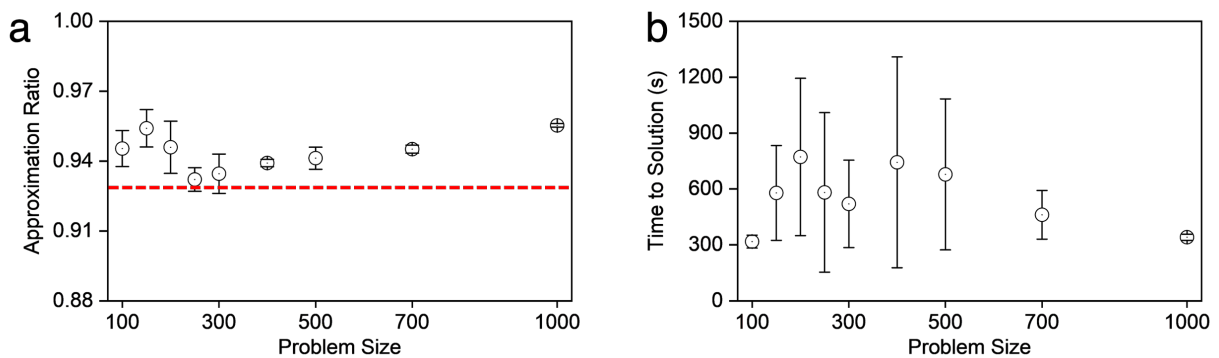


Figure S10: Scalability of our quantum algorithm. Approximation ratio (a) and time to solution (b) of DVQOA as a function of n (≥ 100). The algorithm demonstrates stable performance with approximation ratios over 0.93 (red dash line), even for large-scale Max-Cut problems that are intractable for previous approaches.

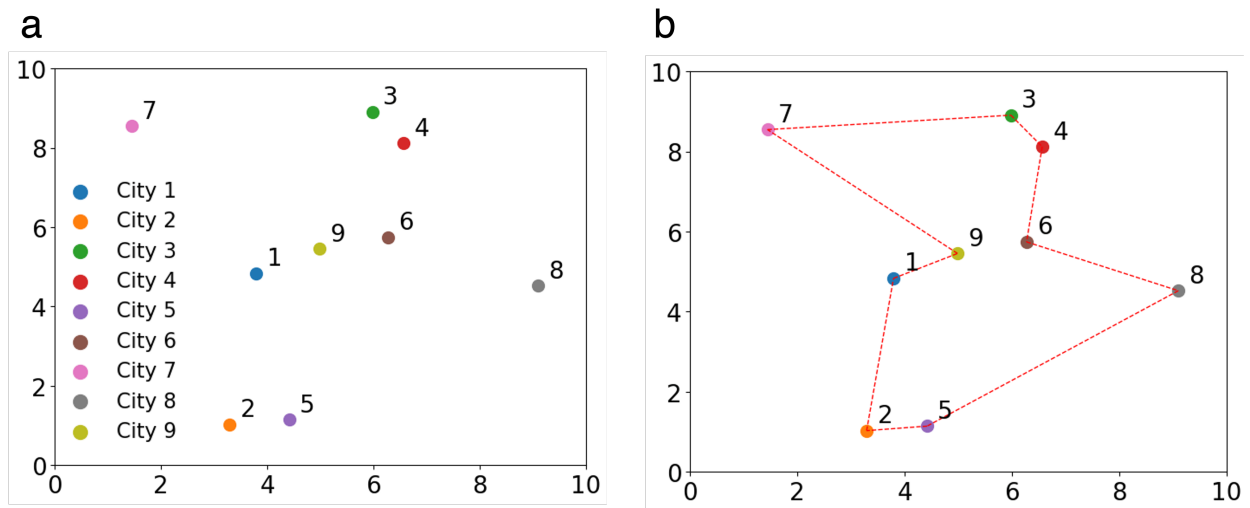


Figure S11: TSP. **a**, Schematic representation of a traveling salesman problem with 9 cities, each represented by colored circles. **b**, The optimal solution that minimizes the total travel path, highlighted by the red dotted line.

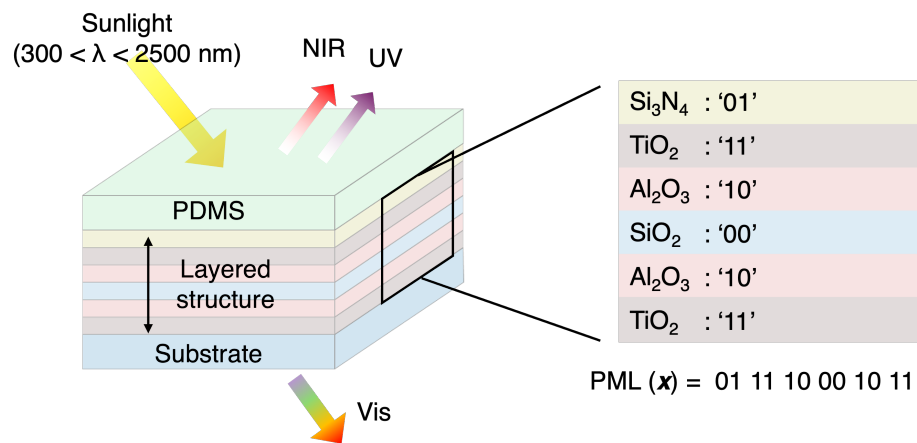


Figure S12: Layered photonic structures for energy-saving window applications. Schematic representation of a layered photonic structure, where each layer is selected from one of four material candidates. Ideally, within the solar spectrum (300 nm <math>< \lambda</math> <math>< 2,500</math> nm), the photonic structure reflects UV and NIR photons while transmitting visible photons, allowing solar irradiance to pass only in the visible spectrum. Additionally, the photonic structure can function as a transparent radiative cooler by incorporating a thin thermal-radiative polymer layer on the top, enabling thermal radiation emission through an atmospheric window (8 μm <math>< \lambda</math> <math>< 13</math> μm).

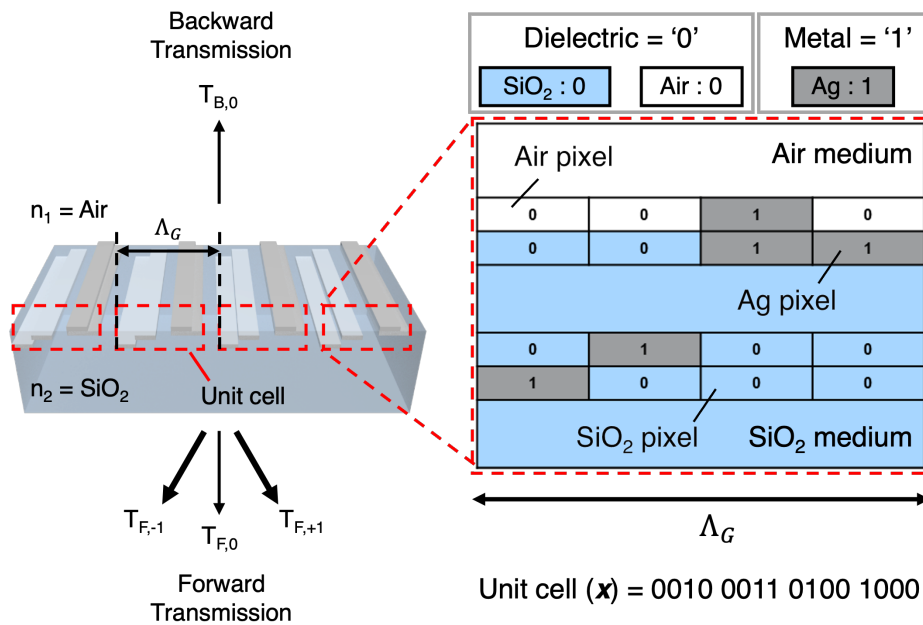


Figure S13: Metamaterial optical diodes. Schematic representation of a pixelated metamaterial optical diode, where each pixel is composed of either dielectric or metallic materials. The unit cell configuration critically influences the optical diode's performance. Ideally, forward transmission (T_F) should be close to 1 while backward transmission (T_B) should be close to 0, resulting in a low FOM (approaching -1).

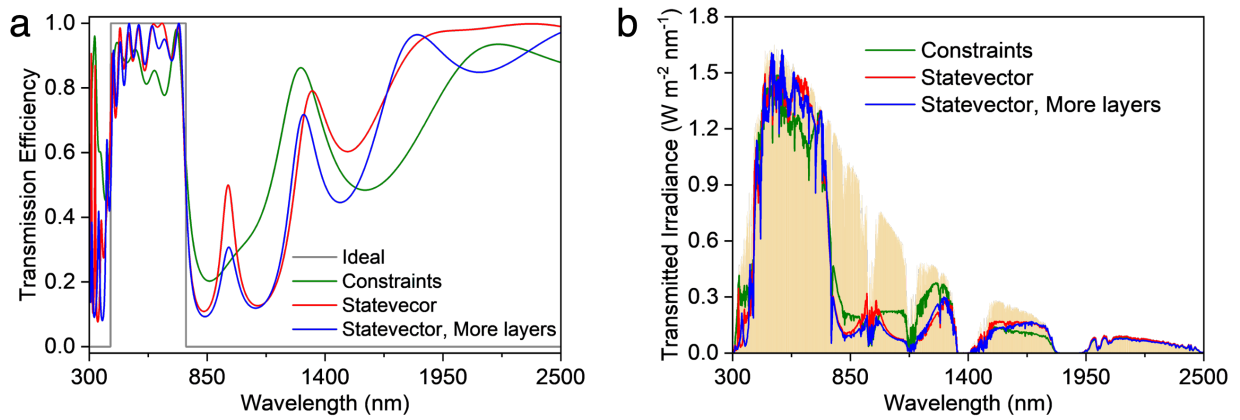


Figure S14: Optical characteristics of the optimized photonic structures. Transmission efficiency (a) and transmitted irradiance (b) of the optimized structures using DVQOA with additional qubits and constraints, the state vector representation, and the state vector representation with enhanced hyperparameters (i.e., more layers). The state vector representation with enhanced hyperparameters demonstrates superior performance.

Supplementary Tables

Table S1: Performance demonstration of HQA for Max-Cut problems. HQA effectively identifies solutions that are optimal, slightly better, or slightly worse compared to the best-known solutions, showing its exceptional performance in solving Max-Cut problems. Hence, results obtained from HQA are used as references to calculate approximation ratios for large-scale problems.

Instances	# Nodes	# Edges	Best Known	HQA	Error (%)
G14	800	4,694	-3,064	-3,064	0
G15	800	4,661	-3,050	-3,050	0
G22	2,000	19,990	-13,359	-13,359	0
G49	3,000	6,000	-6,000	-6,000	0
G50	3,000	6,000	-5,880	-5,878	-0.0340
G55	5,000	12,468	-10,294	-10,283	-0.1068
G70	10,000	9,999	-9,541	-9,543	+0.0209

Table S2: Performance analysis for TSP. DVQOA identifies (near)-optimal routes with short distances, outperforming a classical solver (SA) and achieving performance comparable to a leading quantum solver in this field (HQA). These results highlight its reliable efficiency and reliability in solving route optimization problems.

Number of cities	4	5	6	7	8	9
SA Distance	15.1176	26.4967	37.2334	43.8858	39.4190	39.4103
HQA Distance	15.1176	25.5257	24.8743	24.6725	25.7260	22.8354
DVQAO Distance	15.1176	25.5257	24.8743	24.6725	25.7260	23.3350
Shortest Distance	15.1176	25.5257	24.8743	24.6725	25.7260	22.6863

Table S3: Performance comparison between DVQOA and DDNN. DVQOA consistently identifies lower-valued solutions with significantly shorter time-to-solution compared to DDNN, highlighting its superior efficiency and performance. $Pk-n$: k is the order of interaction and n is the problem size.

Instances	P3-40	P4-40	P5-28	P5-30	P5-33	P5-36
DVQOA Solution	-128.335	-610.677	-498.184	-521.806	-763.639	-996.808
DVQOA Time to Solution (s)	1,002.02	1,360.72	832.014	1,087.63	1,627.33	2,570.82
DDNN Solution	-128.335	-610.676	-498.184	-521.806	-740.253	-992.042
DDNN Time to Solution (s)	1,206.41	15,924.7	20,025.8	28,824.4	46,137.0	72,940.1
Acceleration	1.20398	11.7031	24.0690	26.5020	28.3512	28.3723

Table S4: Performance of DVQOA for higher-order (k^{th}), ternary ($N = 3$) optimization problems. Approximation ratio and time to solution achieved by DVQOA for ternary optimization problems with different n and k . Ternary problems present exponentially larger solution spaces compared to binary problems (3^n vs. 2^n). However, DVQOA efficiently identifies the ground truth solution with linear complexity for n , offering substantial acceleration over brute force search. Higher hyperparameter values (n and $k = 7$, instead of 3) are applied for more complex problems ($n-k$: 16-3, 18-2, 18-3, 20-2, and 20-3).

n	10		12		14	
k	2	3	2	3	2	3
Approximation Ratio	1	1	1	1	1	1
Time to Solution (s)	5.1720	4.8447	6.2711	7.0768	8.2166	9.3404
Brute Force Time (s)	9.7903	33.1126	124.989	505.865	1,511.21	4,706.11
n	16		18		20	
k	2	3	2	3	2	3
Approximation Ratio	1	1	1	1	1	1
Time to Solution (s)	13.4553	68.4385	85.4075	85.6456	108.070	80.0101
Brute Force Time (s)	34,638.7	177,079	386,275	2,356,129	5,573,068	21,294,785

Table S5: Importance of hyperparameter tuning for complex problems in DVQOA. Approximation ratio and time to solution achieved by DVQOA for ternary optimization problems with smaller hyperparameter values (n and $k = 3$) for complex problems ($n-k$: 16-3, 18-2, 18-3, 20-2, and 20-3). While DVQOA shows fast time to solution with smaller hyperparameters, it fails to achieve an approximation ratio of 1, highlighting the importance of tuning hyperparameters for complex problems to identify high-quality solutions. Hence, higher hyperparameter values are recommended for achieving higher solution accuracy in such cases.

n	16		18		20	
k	2	3	2	3	2	3
Approximation Ratio	1	0.9951	0.9689	0.9541	0.9895	0.9632
Time to Solution (s)	13.4553	12.2193	13.4169	14.9551	19.2309	18.7308
Brute Force Time (s)	34,638.7	177,079	386,275	2,356,129	5,573,068	21,294,785

References

49. M. Zaman, K. Tanahashi, S. Tanaka, PyQUBO: Python library for mapping combinatorial optimization problems to QUBO form. *IEEE Transactions on Computers* 71 (4), 838–850 (2021).
50. H. Irie, H. Liang, T. Doi, S. Gongyo, T. Hatsuda, Hybrid quantum annealing via molecular dynamics. *Scientific reports* 11 (1), 8426 (2021).
51. S. Kim, S. Jung, A. Bobbitt, E. Lee, T. Luo, Wide-angle spectral filter for energy-saving windows designed by quantum annealing-enhanced active learning. *Cell Reports Physical Science* 5 (3) (2024).
52. J. Li, et al., Ultrathin, soft, radiative cooling interfaces for advanced thermal management in skin electronics. *Science advances* 9 (14), eadg1837 (2023).
53. J. Li, et al., A tandem radiative/evaporative cooler for weather-insensitive and high-performance daytime passive cooling. *Science Advances* 8 (31), eabq0411 (2022).
54. A. Luce, A. Mahdavi, F. Marquardt, H. Wankerl, TMM-Fast, a transfer matrix computation package for multilayer thin-film optimization: tutorial. *JOSA A* 39 (6), 1007–1013 (2022).
55. B. Shen, R. Polson, R. Menon, Integrated digital metamaterials enables ultra-compact optical diodes. *Optics Express* 23 (8), 10847–10855 (2015).
56. B. Tang, Z. Li, Z. Liu, F. Callewaert, K. Aydin, Broadband asymmetric light transmission through tapered metallic gratings at visible frequencies. *Scientific reports* 6 (1), 39166 (2016).
57. Y. Kim, et al., Meent: Differentiable Electromagnetic Simulator for Machine Learning. arXiv preprint arXiv:2406.12904 (2024).
58. G. Buonaiuto, F. Gargiulo, G. De Pietro, M. Esposito, M. Pota, The effects of quantum hardware properties on the performances of variational quantum learning algorithms. *Quantum Machine Intelligence* 6 (1), 9 (2024).
59. L. K. Grover, The advantages of superposition. *Science* 280 (5361), 228–228 (1998).
60. A. Mandal, A. Roy, S. Upadhyay, H. Ushijima-Mwesigwa, Compressed quadratization of higher order binary optimization problems, in *Proceedings of the 17th ACM International Conference on Computing Frontiers* (2020), pp. 126–131